Neuroradiology (2003) 45: 404–409
DOI 10.1007/s00234-002-0922-8

M. Piotin
P. Gailloud
L. Bidaut
S. Mandai
M. Muster
J. Moret
D.A. Rüfenacht

CT angiography, MR angiography and rotational digital subtraction angiography for volumetric assessment of intracranial aneurysms. An experimental study

Received: 20 February 2002
Accepted: 16 November 2002
Published online: 26 April 2003

M. Piotin (✉) · J. Moret
Service de Neuroradiologie Interventionnelle, Hôpital de la Fondation Rothschild, 25–29 rue Manin, 75940 Paris Cedex 19, France
E-mail: mpiotin@fo-rothschild.fr
Tel.: +33-1-48036833
Fax: +33-1-48036834

M. Piotin · P. Gailloud · S. Mandai
M. Muster · D.A. Rüfenacht
Department of Radiology, University Hospital of Geneva, Geneva, Switzerland

L. Bidaut
Laboratory of Functional and Multidimensional Imaging, University Hospital of Geneva, Geneva, Switzerland

Abstract The purpose of our experimental study was to assess the accuracy and precision of CT angiography (CTA), MR angiography (MRA) and rotational digital subtraction angiography (DSA) for measuring the volume of an in vitro aneurysm model. A rigid model of the anterior cerebral circulation harbouring an anterior communicating aneurysm was connected to a pulsatile circuit. It was studied using unenhanced 3D time-of-flight MRA, contrast-enhanced CTA and rotational DSA angiography. The source images were then postprocessed on dedicated workstations to calculate the volume of the aneurysm. CTA was more accurate than MRA ($P = 0.0019$). Rotational DSA was more accurate than CTA, although the difference did not reach statistical significance ($P = 0.1605$), and significantly more accurate than MRA ($P < 0.00001$). CTA was more precise than MRA ($P = 0.12$), although this did not reach statistical significance. Rotational DSA can be part of the diagnosis, treatment planning and support endovascular treatment of intracranial aneurysms. The emerging endovascular treatment techniques which consist of using liquid polymers as implants to exclude aneurysms from arterial circulation would certainly benefit from this precise measurement of the volume of aneurysms.

Keywords Intracranial aneurysm · Endovascular therapy · Cerebral angiography · Computed tomographic angiography · Magnetic resonance angiography

Introduction

Endovascular techniques include the use of coils as implants to occlude ruptured saccular aneurysms. Since density of coil packing has been shown to be critical for long-term circulatory exclusion of these lesions, techniques using implants might benefit from exact quantification of the volume of the aneurysm to guide the intervention. Other filling materials, such as liquid polymers, are emerging as alternatives to coils to obtain better filling of the aneurysm sac [1, 2, 3, 4, 5, 6]. These methods may critically depend on proper assessment of the volume of the aneurysm prior to embolisation. CT angiography (CTA) and MR angiography (MRA) have gained acceptance as screening tests to detect and demonstrate ruptured and unruptured intracranial aneurysms [7, 8, 9, 10]. Digital subtraction angiography (DSA) with three-dimensional reconstruction has shown to be very effective in planning endovascular or surgical treatment of aneurysms [11, 12, 13, 14]. There has been no report of the potential usefulness of imaging for measuring the volume of aneurysms prior to treatment. Our aim was to assess the accuracy and precision of CTA, MRA and 3D DSA for this task, using an in vitro aneurysm model.

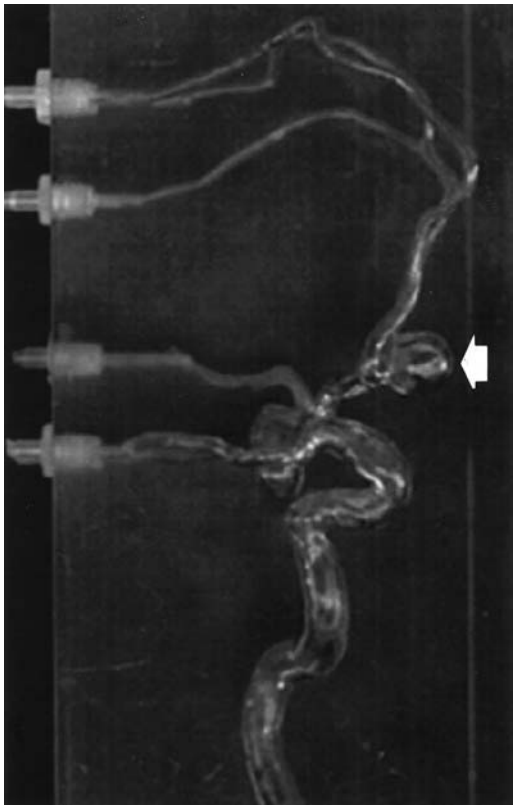

Fig. 1 Vascular model consisting of a hollow, transparent epoxy block spanning an anterior communicating artery aneurysm (*arrow*)

Materials and methods

We used an anatomically correct vascular phantom mimicking the cerebral anterior circulation, created from human vascular moulds by the lost-wax technique [15]. The initial model was obtained from postmortem casting of human vascular segments by injecting plastic resin into the internal carotid artery of a cadaver prior to corrosion of all surrounding biological tissues. The plastic mould of the vessel lumen was then simplified and modified. We added an anterior communicating artery (ACoA) aneurysm after simplification of the arterial tree. Using standard dentistry techniques, we produced exactly identical wax copies of the initial model. Construction of the final model involved embedding the wax model in epoxy resin, which produces a solid transparent block. After melting the encased wax, a hollow in vitro model of a complete segment was obtained. We used a rigid epoxy model which spanned the right internal carotid to the anterior cerebral arteries, onto which we grafted an ACoA aneurysm (Fig. 1).

We developed a micropump capable of injecting very small amounts of liquid with an accuracy of 1.0 ng/ml to measure the volume of the aneurysm precisely. We measured the volume of the aneurysm with the parent artery horizontal and the dome of the aneurysm vertical, so that the orifice of the aneurysm was horizontal. We placed a microcatheter in the model so that its tip was just at the orifice, we filled the sac with contrast medium under fluoroscopic control until the surface of the fluid was just at the level of the orifice. We repeated this procedure five times, and took the average as the definitive volume. We used a cardiac surgery pump to mimic in vivo flow characteristics, with a systolic/diastolic waveform. Arterial flow was simulated with saline solution maintained at 37 °C with a thermistor. The desired flow wave form was specified according to Doppler sonographic measurements of the internal carotid artery, obtaining realistic, reproducible pulsatile flow.

Unenhanced MRA was carried out on this model, with saline circulating within it. Images were acquired using a quadrature head coil in a 1.5 tesla imager. We acquired a volume data-set of the model using a 3D time-of-flight (TOF) sequence with flow compensation and a standard three-excitation gradient-echo technique, flip angle 30 °, repetition time 50 ms, echo time 4 ms, field of view 20 cm, matrix 256×256, slice thickness 0.8 mm with 0.8 mm gap for a total of 90 slices. The source images were acquired in the axial plane, perpendicular to the long axis of the cervical internal carotid artery.

For CTA we injected 40 ml iohexol 300 into the circuit at 1.0 ml/s, using an automatic injector, through a three-way stopcock connected to the outflow pipe of the circuit simulating venous drainage. This slow injection technique, which ensured complete mixing of contrast medium at the level of the aneurysm, provided conditions close to those encountered in patients during helical CT synchronised with the injection. CTA was acquired with optimised helical parameters (collimation 1.5 mm, pitch 1:1, field of view 16 cm, 130 kV/125 mA). The edge-reconstruction kernel had a 512×512 matrix. The reconstruction interval for the images was 1 mm.

Our angiographic setup had a rotational angiography system on a motorised C-arm. A complete acquisition consisted of two rotational scans, covering 180 °, which were combined through acquisition of masks, and image acquisition during the passage of a contrast-medium. We injected 10 ml iohexol 300 using an automatic injector, at 2 ml/s, through a 5 F catheter in the internal carotid artery, providing conditions close to those encountered in clinical examinations. The model was placed on the angiographic table so that it was isocentered to the x-ray source and the image intensifier. The data-set contained 100 acquisition images (angular views) covering 180 °, with a maximum rotation speed of 30°/s, frame rate 12.5 images/s. Each image corresponded to a rotation angle of the whole acquisition system between −90 ° and +90 °. The x-ray acquisition parameters were derived from standard practice: the current (at least 10 mA) and the acceleration potential between 60 and 90 kV with a 10 ms maximum pulse rate were automatically adjusted. Mask and contrast-enhanced images were acquired by consecutive rotations in the same direction. The image intensifier had a diameter of 25 cm and was 1.20 m from the source; the resulting focal spot was 0.3 mm.

CTA source images were postprocessed on a workstation. The aneurysm was segmented in 12 contiguous slices whose area was determined using the full-width at half-maximum above background greyscale thresholding technique to standardise the images (Fig. 2). MRA source images were postprocessed on a workstation to acquire volume measurements. The aneurysm was segmented in 15 contiguous slices whose area was measured in a similar way (Fig. 3). One neuroradiologist (M.P.) performed five volume assessments for both CTA and MRA. Planimetric measurements of each source image of the aneurysm were carried out manually on the workstations after the images were magnified by a factor of 8, without interpolation. The edge of the aneurysm was determined subjectively. The area of the images (number of pixels multiplied by the area of each within the aneurysm) was multiplied by the slice thickness to obtain the volume of the aneurysm. Pixel size for MRA was 0.7812×0.7812 mm, that of CTA 0.3125×0.3125 mm.

For 3D DSA the 100 mask and 100 injected images were postprocessed on a dedicated workstation. We used Feldkamp's algorithm to reconstruct 3D images of the aneurysm (Fig. 4). We used data-sets corrected for geometric distortion with the help of the geometrical parameters extracted from calibration acquisitions performed before the phantom acquisitions [2, 3]. Because direct

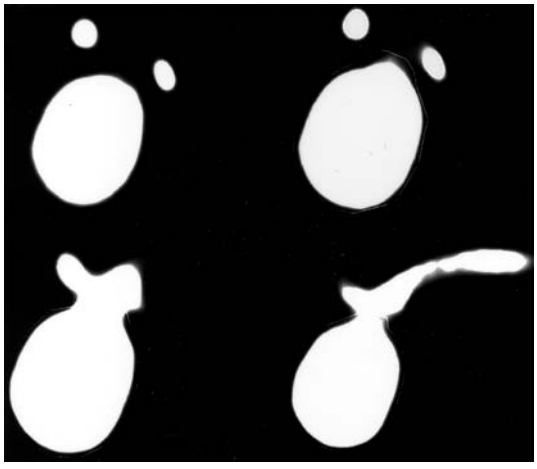

Fig. 2 Source images of CT angiography. Reconstruction of the margin of the aneurysm is sharp, in keeping with the kernel used. The elementary pixel size was 0.3125×0.3125 mm

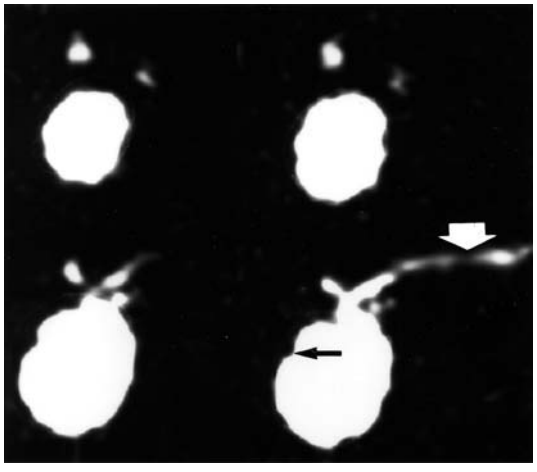

Fig. 3 Source image of MR angiography. Signal drop out in vessels running in-plane is evident (*arrow*). Some signal loss due to disturbed or slow flow is also seen at the periphery of the aneurysm (*arrowheads*). The elementary pixel size was 0.7812×0.7812 mm

correction of the acquisition images mainly eliminated the pincushion effect and the influence of external magnetic fields on the image intensifier and analogue video converter, the other calibration parameters were passed on to the reconstruction program. They helped later in characterising the acquisition geometry for each of the projection images so that these images would be properly handled during reconstruction. Finally, as data were acquired in a realistic way (injection, flow, and rotation), we also needed to correct the individual projections so that, for example, the density of the structures of interest was comparable on all of them. Physical limitations of real blood flow and injection characteristics, as well as the automatic adjustment of the x-ray acquisition parameters to comply with dose requirements, led to a collection of images with variable contrast across a single rotational data set. Each resulting projection image was postprocessed with a global histogram so that the equalisation of each projection image appeared similar in every image of the rotational data set. To extract the aneurysm, we used a combination of thresholding and

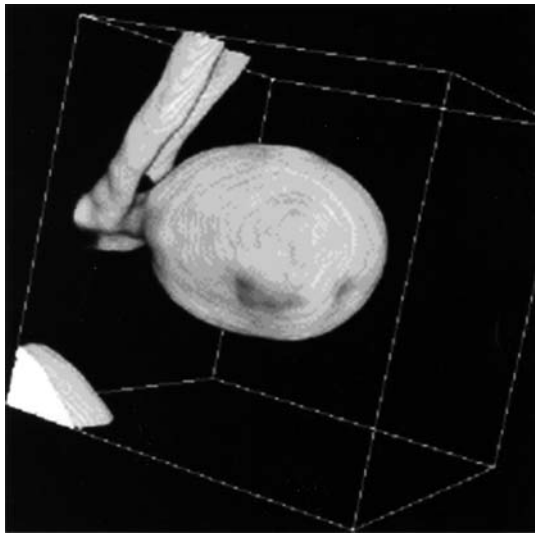

Fig. 4 3D representation of the aneurysm extracted from rotational digital subtraction angiography data. The elementary voxel volume was .23 mm^3

morphotopological techniques which automatically extract the largest connected object from the reconstructed volume [16]. The volume of the aneurysm model was calculated by multiplying the total number of voxels belonging to the segmented aneurysm by the corresponding voxel volume (0.23 mm^3).

CTA and MRA volume measurements were performed by the same operator (M.P.) who delineated the contour of the aneurysm sac manually on the source images. The operations were carried out five times and the average taken for each modality. The volumes obtained by CTA, MRA angiography and 3D DSA were compared with that obtained using the micropump injector, and the average difference and standard deviations (SD) were obtained. Accuracy (the difference between calculated and actual volumes) of the modalities was compared using the Student's *t* test. Precision (the variance of the measured from the actual volume) was compared by the F test of variance. The level of statistical significance was $P \leq 0.05$.

Results

On CT, the epoxy model had a uniform density of 107 Hounsfield units (HU); this figure was obtained after 32 measurements of the region of interest (the aneurysm) before injection of contrast medium. The SD (± 3 HU) reflected background noise. The flow dynamics were shown by the pulsatile wave form seen on Doppler sonography of the model's internal carotid artery (Fig. 5). 3D images obtained after maximum-intensity projection reconstruction with the model connected to the pulsatile circulating circuit indicated its anatomical accuracy.

The calculated volumes of the aneurysm were 751 mm^3 with 3D DSA, an overestimation of 7%, 782.4 mm^3 with CTA, an overestimation of 11.3%, and 597.4 mm^3 with MRA, an underestimation of 15% (Table 1). CTA was thus more accurate than MRA

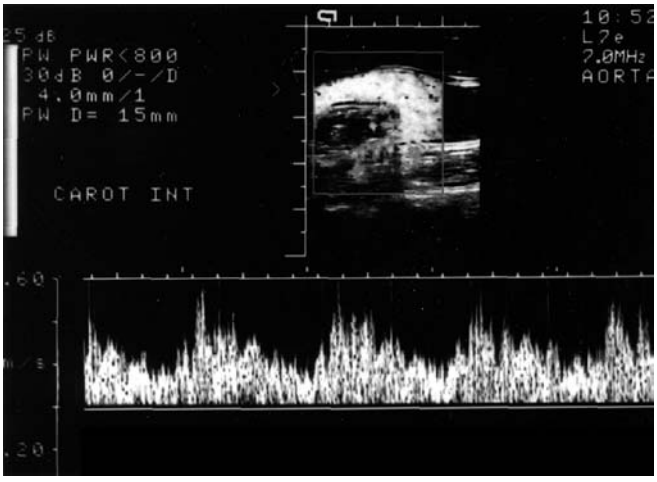

Fig. 5 Doppler sonography of the model at the origin of the internal carotid artery showing systolic/diastolic pattern of flow

($P = 0.0019$) and DSA more accurate than CTA, although the later difference did not reach statistical significance ($P = 0.1605$); DSA was, however, significantly more accurate than MRA ($P < 0.0001$). CTA was more precise than MRA ($P = 0.12$), although again this did not reach statistical significance. Since 3D DSA volume measurement did not require manual intervention, we were unable to compare its precision with that of the other modalities. Intraobserver variability, as reflected by the SD of measurements, was 5% with CTA and 2.8% with MRA.

Discussion

Coiling has gained acceptance and has become the procedure of first choice in some institutions for treatment of aneurysms [17, 18]. The use of liquid embolic polymers to occlude the aneurysm is a potential alternative and, as a consequence, volumetric assessment of the aneurysm could be valuable.

Using an in vitro model permits multiple acquisitions with different imaging modalities; this would be difficult in animal models. Although models derived from injection casting of cadavers have been described [19], our approach is a flexible technique which can be used to produce fully three-dimensional vascular phantoms. Its advantage is that the true geometry of the arterial tree is reproducible and anatomically adequate; many identical copies of the same model can be produced [15]. We chose to use epoxy resin; the models are therefore robust and stable, as well as being compatible with x-ray and MRI techniques. The lost-wax technique allows one to obtain many anatomically identical copies of the anterior cerebral circulation of a human cadaver; the one we used had asymmetrical A1 segments, a situation known to favour the development of an ACoA aneurysm [20]. The potential pitfall of a rigid model like ours is the lack of vessel elasticity and pulsatility. Nevertheless, this had little effect on flow velocities; vessel elasticity has no major influence on the average flow velocity within aneurysms [21]. A second limitation is that the aneurysms we formed were not "true" anatomical ones. They were probably much more regular in shape than intracranial aneurysms encountered in vivo. For image acquisition, our model was connected to a circulation circuit with a pulsatile pump to simulate arterial flow. Realistic pulsatile flow rates were obtained and used in a reproducible manner and the measurements were precise. Nevertheless, the saline solution we used did not reproduce the rheological conditions in vivo since its viscosity did not match that of blood. Because we were dealing with a clearly delineated rigid model, partial-volume effects due to pulsatile motion or others causes were not as marked as they would have been with true in-vivo acquisitions.

Reconstruction of the margins of the aneurysm with CTA was surprisingly good, considering the pulsatile nature of the flow, which might have resulted in a time-varying iodine concentration within the aneurysm during acquisition of the source image. CTA reflects the volume of contrast medium in a structure and appears to be independent of flow rate, and we did not encounter flow-related artefacts. This gave better demonstration of the margins of the aneurysm. Differences in localising the neck on the source images of the aneurysm should not have accounted for the discrepancy between CTA and MRA volumes since these operations were carried out by the same operator and averaged by repeating the procedure five times. The pixel segmentation method used for CTA and MRA was a simple graphical approach which required manual intervention to delineate

Table 1 Measurements (mm^3) of aneurysm with the three imaging modalities

Technique	Measurement					Mean ± SD	Percentage of true volume
	1	2	3	4	5		
CT angiography	817	752	808	726	809	782.4 ± 40.8	111
MR angiography	587	602	594	624	580	597.4 ± 17	85
Digital subtraction angiography	751	–	–	–	–	751	107

the margins of the aneurysm. Despite the repetitions used to reduce potential errors in measurement, we showed that the 3D DSA seems to have a quantitative edge over CTA and MRA. Most clinical projects on CTA of intracranial aneurysms have used narrow collimation as we did, usually between 1 and 2 mm. This improves detection of small aneurysms, while pitch values up to 1.5:1 can be used without significantly decreasing diagnostic accuracy. In a previous in vitro study, diagnostic accuracy was improved by narrow collimation of 1.5 mm [22]. We increased the pitch from 1:1 to 1.5:1 to conserve good longitudinal coverage without changing the clinical accuracy. We found a statistically significant change in the error of volume measurements. The more accurate measurements obtained with 3D DSA can be explained in part by partial volume effects on CTA and MRA, which could have led to a systematic error. If a pixel included portions of both the aneurysm and the epoxy wall of the model, the resultant pixel density on the workstation screen would have been a weighted average of their densities. Previous CTA studies have suggested that the use of a level halfway between the intraluminal and mural densities yielded the most accurate demonstration of a vascular model [23]. A higher threshold would have decreased and a lower one increased the apparent size of the vessel. Widening the window would have increased the apparent size. Automated computer measurement of the edge and volume of the aneurysm would have been preferable to the subjective manual method we used and reduced intraobserver variability, but the software was not available to us. The threshold chosen for measurement would still have been critical but we would have gained in precision. The potential for obscuring an aneurysm due to the similarities in attenuation of blood and contrast medium exists with CTA angiography in the acute stage of subarachnoid haemorrhage.

Both phase-contrast (PC) and TOF MRA techniques have been demonstrated to be of value in providing 2D and 3D images of aneurysms. However, both have limited anatomical coverage and cannot consistently reveal regions of slow flow. This remains a significant challenge for routine MRA. TOF MRA is still limited in demonstration of minute, complex vascular anatomy as an intracranial aneurysm may not be appreciated because of loss of signal from saturation effects or dephasing due to slow or complex flow [24]. Spins travelling in-plane might cause signal drop out in the sac. Prior studies have demonstrated that flow-related artefacts result in underestimation of the size of aneurysms more than 1.5 cm in diameter, particularly if TOF or PC sequences with high velocity-encoding values are used [25, 26]. Schwartz et al. [7] reported that smaller aneurysms (3–5 mm) may be poorly seen on MRA, owing to slow blood flow within them. In vivo, local susceptibility artefacts from aneurysm clips or coils from previous treatment may reduce signal from vessels. Interpretation of TOF MRA must take account of potential pitfalls, which can be minimised by adoption of appropriate imaging and review strategies. This requires careful consideration of source data. Multiple overlapping thin-slab acquisition TOF MRA allows greater coverage, a higher signal-to-noise ratio and higher resolution than conventional MRA. However, it suffers from slab boundary artefacts (“Venetian blind artefacts”), a major limitation. A refinement is the “SLINKY” technique, which eliminates slab boundary artefacts by suppressing them as a series of ghosts. It also produces flow-related signal enhancement, insensitive to the direction of blood flow [27]. This refinement was not available to us.

Another potential pitfall of MRA is in the assessment of acutely ruptured intracranial aneurysms. TOF methods have significant limitations because haemoglobin breakdown products, which occur soon after the haemorrhage, impair accurate demonstration of vascular anatomy and cause blurring of the aneurysm. In the acute stage, the patient may be too unstable to cooperate for the time required for MRA. Methaemoglobin has a very short T1 and, because TOF MRA effectively produces T1-weighted images, early subacute haematomas in the basal cisterns produce strong signals unrelated to flow, decreasing the accuracy of the technique.

Although our 3D DSA results appeared very promising, clinically relevant issues might decrease the quality of the reconstruction in vivo. The data used when reconstructing the aneurysm came from a difference between the mask and images obtained with contrast medium. In the model the later is flowing along with the saline and diluting in the saline pool at the same time as equipment rotation takes place for image acquisition. These 3D reconstruction techniques work best when all projection data represent the same object from various angles. In vivo the contrast medium is not injected instantaneously, the heart beats several times during the rotation, and the contrast medium is diluted while the blood flows. To compensate partially for these problems, projection data must be preprocessed to increase the contrast of the vessels while restoring a comparable dynamic range for all projections. Because our model was rigid, this did not result in degradation of the data caused by the inhomogeneity of the surrounding tissues or the motion of the vascular tree caused by the pulsatile flow during acquisition. Such degradation generally produces blurring of the data, which results in more difficult segmentation of the structure of interest such as an aneurysm.

References

1. Sugiu K, Kinugasa K, Mandai S, Tokunaga K, Ohmoto T (1995) Direct thrombosis of experimental aneurysms with cellulose acetate polymer (CAP): technical aspects, angiographic follow up, and histological study. J Neurosurg 83: 531–538
2. Piotin M, Mandai S, Sugiu K, Gailloud P, Rüfenacht DA (2001) Endovascular treatment of cerebral aneurysms: an in vitro study with detachable platinum coils and tricellulose acetate polymer. Am J Roentgenol 176: 235–239
3. Nishi S, Taki W, Nakahara I, et al (1996) Embolization of cerebral aneurysms with a liquid embolus, EVAL mixture: report of three cases. Acta Neurochir (Wien) 138: 294–300
4. Murayama Y, Vinuela F, Tateshima S, Vinuela F Jr, Akiba Y (2000) Endovascular treatment of experimental aneurysms by use of a combination of liquid embolic agents and protective devices. AJNR 21: 1726–1735
5. Kinugasa K, Mandai S, Tsuchida S, et al (1994) Cellulose acetate polymer thrombosis for the emergency treatment of aneurysms: angiographic findings, clinical experience, and histopathological study. Neurosurgery 34: 694–701
6. Kinugasa K, Mandai S, Terai Y, Kamata I, et al (1992) Direct thrombosis of aneurysms with cellulose acetate polymer. Part II: Preliminary clinical experience. J Neurosurg 77: 501–507
7. Schwartz RB, Tice HM, Hooten SM, Hsu L, Stieg PE (1994) Evaluation of cerebral aneurysms with helical CT: correlation with conventional angiography and MR angiography. Radiology 192: 717–722
8. Vieco PT, Shuman WP, Alsofrom GF, Gross CE (1995) Detection of circle of Willis aneurysms in patients with acute subarachnoid hemorrhage: a comparison of CT angiography and digital subtraction angiography. Am J Roentgenol 165: 425–430
9. Villablanca JP, Martin N, Jahan R, et al (2000) Volume-rendered helical computerized tomography angiography in the detection and characterization of intracranial aneurysms. J Neurosurg 93: 254–264
10. Atlas SW, Sheppard L, Goldberg HI, Hurst RW, Listerud J, Flamm E (1997) Intracranial aneurysms: detection and characterization with MR angiography with use of an advanced postprocessing technique in a blinded-reader study. Radiology 203: 807–814
11. Tanoue S, Kiyosue H, Kenai H, Nakamura T, Yamashita M, Mori H (2000) Three-dimensional reconstructed images after rotational angiography in the evaluation of intracranial aneurysms: surgical correlation. Neurosurgery 47: 866–871
12. Anxionnat R, Bracard S, Ducrocq X, et al (2001) Intracranial aneurysms: clinical value of 3D digital subtraction angiography in the therapeutic decision and endovascular treatment. Radiology 218: 799–808
13. Bidaut LM, Laurent C, Piotin M, et al (1998) Second-generation three-dimensional reconstruction for rotational three-dimensional angiography. Acad Radiol 5: 836–849
14. Missler U, Hundt C, Wiesmann M, Mayer T, Bruckmann H (2000) Three-dimensional reconstructed rotational digital subtraction angiography in planning treatment of intracranial aneurysms. Eur Radiol 10: 564–568
15. Gailloud P, Pray JR, Muster M, Piotin M, Fasel JH, Rüfenacht DA (1997) An in vitro anatomic model of the human cerebral arteries with saccular arterial aneurysms. Surg Radiol Anat 19: 119–121
16. Bidaut LM, Pascual-Marqui R, Delavelle J, et al (1996) Three-to-five-dimensional multisensor imaging for the assessment of neurological (dys)function. J Digit Imaging 9: 185–198
17. Byrne JV, Sohn MJ, Molyneux AJ, Chir B (1999) Five-year experience in using coil embolization for ruptured intracranial aneurysms: outcomes and incidence of late rebleeding. J Neurosurg 90: 656–663
18. Cognard C, Weill A, Spelle L, et al (1999) Long-term angiographic follow-up of 169 intracranial berry aneurysms occluded with detachable coils. Radiology 212: 348–356
19. Kerber CW, Heilman CB, Zanetti PH (1989) Transparent elastic arterial models. I: A brief technical note. Biorheology 26: 1041–1049
20. Kerber CW, Imbesi SG, Knox K (1999) Flow dynamics in a lethal anterior communicating artery aneurysm. AJNR 20: 2000–2003
21. Steiger HJ, Liepsch DW, Poll A, Reulen HJ (1988) Hemodynamic stress in terminal saccular aneurysms: a laser-Doppler study. Heart Vessels 4: 162–169
22. Kallmes DF, Evans AJ, Woodcock RJ, et al (1996) Optimization of parameters for the detection of cerebral aneurysms: CT angiography of a model. Radiology 200: 403–405
23. Dix JE, Evans AJ, Kallmes DF, Sobel AH, Phillips CD (1997) Accuracy and precision of CT angiography in a model of carotid artery bifurcation stenosis. AJNR 18: 409–415
24. Wilcock DJ, Jaspan T, Worthington BS (1995) Problems and pitfalls of 3-D TOF magnetic resonance angiography of the intracranial circulation. Clin Radiol 50: 526–532
25. Pernicone JR, Siebert JE, Potchen EJ, Pera A, Dumoulin CL, Souza SP (1990) Three-dimensional phase-contrast MR angiography in the head and neck: preliminary report. AJNR 11: 457–466
26. Huston J 3rd, Rüfenacht DA, Ehman RL, Wiebers DO (1991) Intracranial aneurysms and vascular malformations: comparison of time-of-flight and phase-contrast MR angiography. Radiology 181: 721–730
27. Liu K, Rutt BK (1998) Sliding interleaved kY (SLINKY) acquisition: a novel 3D MRA technique with suppressed slab boundary artifact. J Magn Reson Imaging 8: 903–911